Generalization of the post-collision interaction effect from gas-phase to solid-state systems demonstrated in thiophene and its polymers

Nicolas Velasquez, Oksana Travnikova, Renaud Guillemin, Iyas Ismail, Loïc Journel, Jessica B Martins, Dimitris Koulentianos, Denis Céolin, Laure Fillaud, Maria Luiza M. Rocco, et al.

Generalization of the post-collision interaction effect from gas-phase to solid-state systems demonstrated in thiophene and its polymers

Nicolas Velasquez [1,*] Oksana Travnikova [1,2] Renaud Guillemin [1,2] Iyas Ismail [1,2] Loïc Journel [1,2] Jessica B. Martins [1,†] Dimitris Koulentianos [1,‡] Denis Céolin [2] Laure Fillaud [3] Maria Luiza M. Rocco [4] Ralph Püttner [5] Maria Novella Piancastelli [1,6] Marc Simon [1,2] Sergei Sheinerman [7] Leonid Gerchikov [8] and Tatiana Marchenko [1,2,§]

[1]*Sorbonne Université, CNRS, Laboratoire de Chimie Physique-Matière et Rayonnement, LCPMR, F-75005 Paris Cedex 05, France*
[2]*Synchrotron Soleil, L'Orme des Merisiers, Saint-Aubin, F-91192 Gif-sur-Yvette, France*
[3]*Sorbonne Université, CNRS, Laboratoire Interfaces et Systèmes Electrochimiques, LISE, F-75005 Paris Cedex 05, France*
[4]*Instituto de Química, Universidade Federal do Rio de Janeiro, 21941-909, Rio de Janeiro, Brazil*
[5]*Fachbereich Physik, Freie Universität Berlin, Arnimallee 14, D-14195 Berlin, Germany*
[6]*Department of Physics and Astronomy, Uppsala University, SE-75120 Uppsala, Sweden*
[7]*Department of Physics, St. Petersburg State Marine Technical University, 190121 St. Petersburg, Russia*
[8]*Department of Physics, Peter the Great St. Petersburg Polytechnic University, 195251 St. Petersburg, Russia*

(Received 3 June 2022; revised 9 September 2022; accepted 2 November 2022; published 26 January 2023)

We demonstrate experimentally and theoretically the presence of the post-collision interaction (PCI) effect in sulfur $KL_{2,3}L_{2,3}$ Auger electron spectra measured in the gas-phase thiophene and in solid-state organic polymers: polythiophene (PT) and poly(3-hexylthiophene-2,5-diyl), commonly known as P3HT. PCI manifests itself through a distortion and a blueshift of the normal Auger S $KL_{2,3}L_{2,3}$ spectrum when S 1*s* ionization occurs close to the ionization threshold. Our investigation shows that the PCI-induced shift of the Auger spectra is stronger in the solid-state polymers than in the gas-phase organic molecule. Theoretical modeling within the framework of the eikonal approximation provides good agreement with the experimental observations. In a solid medium, two effects influence the interaction between the photoelectron and the Auger electron. In detail, stronger PCI in the polymers is attributed to the photoelectron scattering in the solid, which overcompensates the polarization screening of electron charges which causes a reduction of the interaction. Our paper demonstrates the general nature of the PCI effect occurring in different media.

DOI: 10.1103/PhysRevResearch.5.013048

I. INTRODUCTION

The ionization of atomic inner shells leads to the creation of intermediate excited states and their subsequent relaxation via emission of electrons and x-ray photons. The Coulomb interaction between the emitted electrons and the remaining ion noticeably distorts the electron spectra, and this phenomenon is known as the post-collision interaction (PCI) effect. The PCI effect has been thoroughly explored for decades in gas-phase atoms [1,2] and molecules [3–6]. Fewer studies have been performed on PCI in condensed media [7–12].

Meanwhile, understanding the mechanism of PCI and its manifestation in solids is of significant practical interest. Methods such as x-ray photoelectron spectroscopy and Auger electron spectroscopy are widely used in materials science for analysis of surfaces and interfaces of a vast range of materials. The accuracy of these methods strongly relies on the careful description and interpretation of the shape and energy position of the spectral lines, which can be significantly affected by the PCI effect. Aiming at the development of a generalized description of the PCI effect in a variety of media, we have performed a comparative study in gas-phase thiophene and in solid thiophene-based polymers.

An observation of the PCI effect was made in atoms bombarded by slow ions [13,14]. In the following 20 years, the PCI effect was studied in a process of electron-impact excitation of the atomic autoionizing states or in the photoionization of the atomic inner shells followed by the Auger decay. In the latter case, ionization is described by the following two-step process. In the first step, photoabsorption yields a photoelectron and a metastable singly charged ion with an inner-shell vacancy, which in the next step undergoes relaxation through emission of an Auger electron leaving the ion doubly charged.

The PCI effect is reduced in this case to the Coulomb interaction between three charged particles: the emitted photo-

*nicolas.velasquez@sorbonne-universite.fr
†Present address: Advanced Photon Source, Argonne National Laboratory, 9700 S. Cass Ave, Lemont, Illinois 60439, USA.
‡Present address: Center for Free-Electron Laser Science and Department of Physics, Universität Hamburg, Luruper Chaussee 149, 22761 Hamburg, Germany.
§tatiana.marchenko@sorbonne-universite.fr

electron, the Auger electron, and the remaining ionized atom. Their interaction results in energy exchange between the two emitted electrons. Coulomb repulsion between the outgoing fast Auger electron and the slow photoelectron in the field of the residual ion accelerates the former and slows down the latter. In a classical picture, the closer the photoelectron to the ion at the moment of Auger decay, the larger the energy gain of the Auger electron and, consequently, the energy loss of the photoelectron. Thus, close to the ionization threshold, PCI leads to a substantial distortion and energy shift of both the Auger electron and the photoelectron spectral lines.

The PCI effect in isolated atoms has been extensively studied both theoretically and experimentally. On the theoretical side, a number of models describing PCI have been developed on the basis of classical [14,15], semiclassical [16–19], and quantum mechanical [20–22] approaches. On the experimental side, several techniques have been developed, such as photoelectron-ion coincidence spectroscopy [23], Auger electron spectroscopy [24], and multielectron-coincidence spectroscopy [25,26], which allow addressing different aspects of the PCI effect [23–25,27,28].

The first investigations of the PCI effect in molecules made use of ion time-of-flight mass spectroscopy [3] and two-dimensional photoelectron spectroscopy [5]. Later, photoelectron-ion coincidence spectroscopy performed in the gas-phase OCS molecule revealed the hallmark PCI features and showed that the magnitude of the PCI shift depends on the number of electrons emitted during the Auger cascade [6]. In this paper, the theoretical semiclassical approach, originally used for the atomic case, was successfully extended to the molecular case.

For larger and more complex systems, few examples are found in the literature concerning either experimental or theoretical studies [7–11]. These works revealed two competing mechanisms that affect the PCI in the condensed medium, namely, screening of the Coulomb interaction and electron scattering. While screening weakens the Coulomb interaction and, consequently, suppresses PCI, electron scattering reduces the distance that the photoelectron can travel from the ion in the condensed medium before the Auger decay occurs, and therefore enhances PCI in comparison to the case of an isolated atom.

A significant reduction of PCI was observed in metal as opposed to an insulator medium due to a stronger screening of the Coulomb interaction between the charged particles [7]. A suppression of the PCI effect in photoionization of atoms deposited on a metallic substrate was reported in Refs. [8,9]. This observation was attributed to polarization screening of the Coulomb interaction between the charged particles near the metallic surface that was taken into account by the image charges. Furthermore, an investigation of the PCI effect in x-ray photoelectron spectra measured in isolated noble-gas atoms and atomic clusters showed that the PCI effect in the bulk of a cluster is reduced compared to that of an atom [10]. These findings were also explained with the polarization screening of the bulk medium in the clusters.

The influence of electron scattering on PCI processes was theoretically studied for $L_3M_{4,5}M_{4,5}$ Auger spectrum in solid-state copper [11]. Inelastic electron scattering which slows down photoelectron propagation was shown to amplify the PCI effect. Recently, an observation of the PCI effect in KLL Auger spectra of solvated K^+ and Cl^- ions in aqueous solution has been reported [12].

In this paper, we develop a general description of PCI in a condensed medium, thus extending the well-established quantum mechanical description of PCI for an isolated atom; namely, we demonstrate the presence of the PCI effect in sulfur KLL Auger spectra measured for the gas-phase thiophene and in solid-state organic polymers: polythiophene (PT) and poly(3-hexylthiophene-2,5-diyl), commonly known as P3HT. The choice of these conjugated semiconducting polymers is motivated by their promising applications in optoelectronic devices and organic field-effect transistors [29–32]. The advantage of using KLL Auger spectroscopy after S 1*s* ionization for PCI investigation is related to the short lifetime of the S 1*s* core hole and a well-defined high kinetic energy of the Auger electron resulting in a strong three-body interaction of the charged particles. The PCI effect is manifested as a distortion and a blueshift of the normal Auger S KLL spectrum when S 1*s* ionization occurs close to the ionization threshold. Our investigation shows that the PCI-induced shift of the Auger spectra is stronger in the solid-state polymers than in the gas-phase organic molecule.

Our theoretical approach is based on the well-known eikonal approximation [20], which allows incorporating effects of both polarization screening and electron scattering. The model developed within the framework of the eikonal approximation provides good agreement with the experimental observations. The performed analysis demonstrates that the PCI-based energy exchange between the photoelectron and the Auger electron in the polymer medium is qualitatively similar to the case of an isolated atom, although modified by photoelectron scattering and charge screening. We show that electron scattering in the polymer has a stronger effect on the PCI energy shift than the polarization screening, which effectively results in the enhancement of the PCI effect in the considered PT and P3HT polymers compared to the isolated thiophene molecule.

II. THEORETICAL DESCRIPTION

The process of 1*s* shell photoionization of an isolated sulfur atom, followed by KLL Auger decay, can be represented by the following scheme:

$$\gamma + S \rightarrow e_{\rm ph}(E_0 + i\Gamma_a/2) + S^{+*} \rightarrow e_{\rm ph} + e_A + S^{2+}. \quad (1)$$

In the first step, the incident photon γ ionizes the 1*s* shell of the sulfur atom leaving the residual ion S^{+*} in a metastable autoionizing state with the lifetime width of Γ_a= 0.59 eV [33]. Consequently the emitted photoelectron $e_{\rm ph}$ in the intermediate state has the complex energy $E_0 + i\Gamma_a/2$, where $E_0 = E_\gamma - {\rm IP}$ is the excess photon energy, E_γ is the incident photon energy, and IP is the 1*s* shell ionization potential. Note that such a complexity of the particles' energy is usual for the description of two-step processes, which involve the creation and decay of metastable states (see, e.g., Ref. [1]).

In the second step, the intermediate autoionizing state of the S^{+*} ion with $1s^{-1}$ vacancy decays via KLL Auger transition to the doubly charged sulfur ion S^{2+} with two vacancies in the $2p$ shell resulting in emission of the fast, 2.1 keV,

Auger electron e_A. In the present paper, the excess photon energy E_0 ranges from nearly zero at the threshold up to ∼210 eV. This means that the photoelectron energy $E_{\rm ph} \simeq E_0$ is smaller than the Auger electron energy E_A by at least an order of magnitude. Hence, the Auger electron instantly leaves the interaction region at the moment of Auger decay and the photoelectron experiences a sudden change of the ion field from the potential of the singly to doubly charged sulfur ion. Consequently, the photoelectron loses part of its total energy due to the negative change of its potential energy. Note that this photoelectron energy loss is not accepted by the residual ion but transmitted to the outgoing Auger electron. The heavy ion does not participate in the energy exchange due to its huge mass. Thus, the actual force responsible for PCI energy exchange is the Coulomb repulsion between the photoelectron and Auger electron in the course of their recession in the field of the doubly charged ion. The outgoing Auger electron as a faster particle accelerates due to the Coulomb repulsion and gains additional energy while the photoelectron decelerates and loses its energy. This energy exchange distorts the respective energy spectra: redshifting the maximum of the photoelectron line and blueshifting by the same value ΔE the maximum of the Auger electron line.

The focus of the present paper is the PCI-induced energy shift. In the case of an isolated atom, it has been well described within numerous theoretical approaches [1,2]. For our study, we chose the eikonal approximation [20] because it provides a closed analytical expression for the PCI energy shift (here and throughout the paper, we use the CGS-Gaussian system of units):

$$\Delta E = \frac{\Gamma_a}{2\,\hbar}\left(\frac{e^2}{v_{\rm ph}} - \frac{e^2}{|\mathbf{v}_A - \mathbf{v}_{\rm ph}|}\right), \tag{2}$$

where $v_{\rm ph}$ is the photoelectron velocity and $\mathbf{v}_{\rm ph}$ and $\mathbf{v}_A$ denote velocity vectors of the photoelectron and the Auger electron, respectively. On the other hand, the approximation, which has been developed for the case of an isolated atom, can be extended to the case of an atom embedded in the bulk medium by taking into account both the effect of charge screening and the effect of electron scattering.

The only drawback of the approximation is its limited applicability close to the ionization threshold. Equation (2) can be applied if the PCI energy shift is much smaller than the photoelectron energy $\Delta E \ll E_{\rm ph}$ [20] which, according to Eq. (2), means that $E_0 \gg \Gamma_a^{2/3} E_H^{1/3}/2$, where $E_H = 27.2$ eV is the atomic unit of energy. Under this condition, the approximation provides good agreement with experimental observations (see, e.g., Ref. [34]). The better this condition is fulfilled, the higher is the accuracy provided by Eq. (2). For the ionization process considered in Eq. (1), in the case of an isolated sulfur atom, $\Gamma_a^{2/3} E_H^{1/3}/2 \simeq 1$ eV. For the excess energy $E_0 = 10$ eV, Eq. (2) gives the correct PCI energy with accuracy of 96%, whereas for $E_0 = 5$ eV and $E_0 = 1$ eV the accuracy is 90% and 67%, respectively. In the case of a sulfur atom embedded in the polymer, this condition must be adapted as discussed below.

Let us first consider the applicability of the eikonal approximation in the case of a molecule. According to Eq. (2), the PCI energy shift depends on the lifetime width and the electron velocities, i.e., on the excess photon energy, Auger transition energy, and kinematics of the electron emission. In the particular case of the ionization process considered in Eq. (1), the Auger electron is much faster than the photoelectron. Therefore, the first term on the right-hand side of Eq. (2) is the leading one, while the second term with inverse relative velocity of the Auger electron and the photoelectron provides a small contribution. Hence, ΔE depends on two parameters: Γ_a and $v_{\rm ph} = \sqrt{2E_{\rm ph}/m} \simeq \sqrt{2E_0/m}$, where m is the electron mass.

In this case, Eq. (2) for the PCI energy shift has a simple classical interpretation. The negative PCI energy shift of the photoelectron spectrum, $-\Delta E$, equals the sudden change of ionic potential $-e^2/r$ at the moment of the Auger decay, where r denotes the photoelectron distance from the ion. It can be demonstrated [14] that the energy exchange between the two electrons occurs with the largest probability density at time delay $2\hbar/\Gamma_a$ after K-shell ionization when the photoelectron has moved from the ion at the distance $r = 2\hbar v_{\rm ph}/\Gamma_a$. It leads exactly to PCI energy shift $-\Delta E$ given by Eq. (2) at $v_{\rm ph} \ll v_A$. Typically, the distance r, where the PCI energy exchange takes place, is much larger than the Bohr radius, $r \gg a_0 = \hbar^2/me^2$, because of small values of the lifetime width $\Gamma_a \ll E_H$. In our case, even at the excess energy $E_0 = 1$ eV one obtains $r \simeq 25a_0$.

Therefore, in the molecular case, the PCI between the electrons resulting from the atomic inner-shell ionization does not differ from the case of an isolated atom [6]. On the other hand, we consider the S KLL Auger transition between the deep inner atomic shells. It means that the influence of the molecular environment on the widths and energies of the initial and final ionic states can be neglected. That is why we will use Eq. (2) to describe the PCI energy shift of the Auger electrons emitted from the thiophene molecule.

However, in the case of ionization of a sulfur atom within the thiophene polymer, Eq. (2) should be modified. Polarization of the polymer weakens the Coulomb interaction between the residual sulfur ion, the photoelectron, and the Auger electron. This effect can be taken into account by means of polymer dielectric permittivity ε; namely, we will replace the squared electron charges e^2 by their screened values e^2/ε as in Ref. [10].

Generally, the permittivity ε depends on the frequency of the electric field. To properly account for the charge screening, the permittivity needs to be computed over a wide frequency range, which is beyond the scope of the present paper. The relative permittivity values for P3HT and PT reported in literature fluctuate between ∼ 3–7, depending on the measurement method and the sample environment [35–39]. In our experiment, the permittivity can be strongly affected by such factors as heating of the sample by the x-ray beam, electric contact with the sample holder, P3HT film thickness and blending of polythiophene with the conductive graphite powder. Therefore, in our simulations we use permittivity as a fitting parameter and obtain $\varepsilon = 6.5$ for both polymers, which is within the range of values provided in the literature.

Another effect that should be taken into account is electron scattering which affects electron propagation through the solid medium. On the one hand, the photoelectron may lose energy during inelastic scattering processes. On the other

hand, elastic scattering strongly affects the electron trajectory. Such changes in the electron propagation direction effectively reduce the distance that the photoelectron travels in the solid by the time the Auger decay occurs, resulting in amplification of the PCI effect. The electron propagation through the bulk medium is a very well-studied phenomenon. Regardless of the mechanism of electron scattering (intramolecular scattering [40], electron-phonon collisions [41], scattering off structural imperfections of the medium [42], etc.), this process leads to attenuation of the electron beam intensity $I(x) = I_0 \exp(-x/L)$, where x is the electron path and L is the effective attenuation length (EAL).

It should be noted that even in the case of ionization of an isolated atom, the photoelectron propagation is described by the damped wave function $|\psi(r)|^2 \propto \exp(-r\Gamma_a/\hbar v_{\rm ph})$ because of the complexity of the photoelectron energy $E_0 + i\Gamma_a/2$. The eikonal approach employs the time-dependent representation of the electron wave function $\psi(t) \propto \exp(-\Gamma_a t/2\hbar)$ [20]. In the case of photoelectrons propagating through the solid medium, electron scattering reduces the effective attenuation length, i.e., compared to a free atom, the distance between the photoelectron and the ion at the moment of the Auger decay is reduced. This can be described through an additional contribution $\Gamma_d = \hbar\, v_{\rm ph}/L$ to the photoelectron linewidth. Consequently, the effective photoelectron linewidth that should be used within the eikonal approach is given by the sum

$$\Gamma = \Gamma_a + \Gamma_d = \Gamma_a + \frac{\hbar\, v_{\rm ph}}{L}. \tag{3}$$

Similar to the molecular case, the value of the lifetime width Γ_a for atomic sulfur can be used also in the case of polymers due to negligible influence of the molecular environment on the KLL Auger transition rate. The L values corresponding to the EAL could be obtained from theoretical calculations or experimental measurements. To our knowledge, no EAL measurements neither in P3HT nor in PT polymer samples in the range of the photoelectron energies relevant for our experimental conditions have been reported to date. We have therefore used calculated values obtained using the NIST Electron Effective-Attenuation-Length Database tools [43,44]. More details on the calculation of the EAL factors can be found in the Appendix.

Combining the effects of charge screening and electron scattering in the bulk medium, we replace within the eikonal approach all Coulomb potentials e^2/r by the screened ones $e^2/\varepsilon r$ and the atomic lifetime width Γ_a by the effective photoelectron width Γ. With these substitutions, quantum mechanical calculations within the eikonal approach [20] lead to the following expression for the PCI energy shift in nonmetallic medium:

$$\Delta E = \frac{\Gamma}{2\,\hbar\,\varepsilon}\left(\frac{e^2}{v_{\rm ph}} - \frac{e^2}{|\mathbf{v}_A - \mathbf{v}_{\rm ph}|}\right), \tag{4}$$

where the effective photoelectron linewidth Γ is given by the Eq. (3). Applicability condition of the generalized Eq. (4) remains the same as in the case of an isolated atom: $\Delta E \ll E_{\rm ph}$. However, the restriction for the excess energy changes due to the renormalization of the electric charge and the modified photoelectron effective width: $E_0 \gg (\Gamma/\varepsilon)^{2/3} E_H^{1/3}/2$.

Furthermore, if under the experimental conditions the emission direction of the electrons is not fixed, the eikonal PCI energy shift provided by Eq. (2) or Eq. (4) has to be integrated over all the photoelectron and Auger electron emission angles [19–21]. This leads to the final expression for the PCI shift in solid medium,

$$\Delta E = \frac{\Gamma}{2\,\hbar\,\varepsilon}\left(\frac{e^2}{v_{\rm ph}} - \frac{e^2}{v_A}\right), \tag{5}$$

which we apply for our sulfur Auger KLL measurements in P3HT and PT samples.

III. EXPERIMENT

The experiments were performed at the French national synchrotron facility SOLEIL, GALAXIES beamline [45], on the high-resolution HAXPES end station dedicated to hard-x-ray photoelectron spectroscopy [46]. Linearly polarized light is delivered by a U20 undulator and the photon energies are selected by a Si(111) double-crystal monochromator. Incoming electrons are analyzed by a large-acceptance angle EW4000 Scienta hemispherical analyzer, whose lens axis is set parallel to the polarization vector of the incoming beam. A pass energy of 200 eV and a curved slit of 0.3 mm width were used in the experiment. The instrumental resolution was estimated at ∼180 meV and the photon bandwidth δE provided by the beamline was ∼225 meV and ∼380 meV at 2.5 keV and 3.5 keV photon energy, respectively. Note that the photon bandwidth does not contribute to the experimental resolution of the normal Auger spectra.

Pure liquid thiophene was purchased from Sigma Aldrich and was subjected to three freeze-pump-thaw-degassing cycles. Thiophene vapor present in the headspace above the liquid was slowly injected into a gas cell with the use of a microleak valve and kept at a constant pressure of $\sim 10^{-5}$ mbar in the experimental chamber, which was sufficiently low to consider the molecules as isolated.

P3HT purchased from Sigma Aldrich was dissolved in $CHCl_3$ to a concentration of 5 mg/mL and spin coated on an indium-tin-oxide substrate at ∼2000 RPM. The obtained P3HT film was placed on the metal sample holder and kept in place with carbon tape, which also served as a conductor connecting the sample to the metal holder.

The PT sample was prepared as a blend of pure PT powder and graphite powder in approximately equal amounts, both purchased from Sigma Aldrich. Preparation of the blend, denoted as PTC in the following, allowed us to tackle the space-charge buildup, which can shift and distort the energy distribution of the Auger electrons [47]. Equivalent amounts of polythiophene and graphite powders were finely ground together until a homogeneous blend was obtained. The resulting powder was deposited on the carbon tape, ensuring the entire surface was covered, and fixed on the metal sample holder. Additionally, carbon tape was placed along the perimeter of the PTC blend, improving the electric connection between the surface of the sample and the sample holder.

P3HT and PTC samples were placed in the preparation chamber of the HAXPES end station and subsequently transferred to the main chamber. To avoid radiation damage to the

samples, intensity filters were introduced in the beam and the samples were continuously moved during the measurements.

Auger S KLL electron spectra were measured in gas-phase thiophene, P3HT film, and PTC powder blend at the photon energies from 2475 eV to 3500 eV with variable steps, described in the following: A low-excess energy data set, from ∼0 to 5 eV above threshold with an energy step of 0.5 eV. A mid-excess energy data set, from ∼5 to 20 eV above the ionization threshold, with an energy step of 1 eV. A high-excess energy data set from ∼20 to 200 eV above threshold, with an energy step of 10 eV. In addition, two measurements were performed at ∼500 eV and ∼1000 eV above threshold to assert an incident photon energy where the PCI shifts are absent. The electron kinetic energy and the photon energy were calibrated using the argon LMM Auger and argon $2p^{-1}$ and $1s^{-1}$ photoelectron spectra [48,49] measured under the same experimental conditions.

Note that in the gas-phase experiments, the kinetic energy of the detected electron is naturally measured with respect to the vacuum level [50]. However, in solid-state experiments, the electrons ejected from the sample must overcome an additional potential barrier at the surface, known as the sample work function, which results from the energy difference between the vacuum level and the Fermi level (FL). If the sample and the spectrometer are in good electric contact (as is the case in our experiment), an electron exchange between them results in a common FL. The kinetic energy of the electron ejected from the sample and propagating to the analyzer is further modified by the spectrometer work function ϕ_{SP} [50]. In our calibration measurement using the Au $4f_{7/2}$ photo line, we obtained $\phi_{SP} = 4.90(1)$ eV. Therefore, in P3HT and PTC, the electron kinetic energy referenced to the FL is shifted by the latter amount toward higher values with respect to the kinetic energies measured by the spectrometer.

It is convenient to trace the evolution of the PCI energy shift as a function of the excess energy E_0, which is defined above in the atomic case as the difference between the incident photon energy and the S $1s$ IP. Therefore, in the gas-phase measurements, the reference photon energy E_γ^{ref}, where the excess energy $E_0 = 0$ eV, equals the S $1s$ IP.

The S $1s$ IP in thiophene was determined using sulfur $1s$ photoelectron spectra recorded at 2700 eV photon energy. The obtained value IP=2478.6(3) eV is in good agreement with the 2478.4(5) eV value reported in earlier investigations for the gaseous thiophene [51].

In solid samples, the IP, generally measured with respect to the FL, lies below the near edge x-ray absorption fine structure (NEXAFS) features. Therefore, for a consistent comparison to the gas-phase measurements, we define the reference photon energy $E_\gamma^{\rm ref}$ in our solid samples by adding the term value of 5.0(3) eV, found for the first S $1s$ NEXAFS feature in gaseous thiophene [51], to the energy of the equivalent S $1s$ NEXAFS feature in PT [52] and P3HT [53]. The obtained reference photon energy values, where the excess energy $E_0 = 0$ eV, are $E_\gamma^{\rm ref} = 2477.6$ eV for PT and $E_\gamma^{\rm ref} = 2478.2$ eV for P3HT.

To extract the position of the Auger S KLL line as a function of the photon energy, the Auger spectra were fitted using the SPANCF fitting suite for Igor Pro [54]. At photon energies where peak distortion caused by the PCI effect was deemed negligible, the spectra were fitted with Voigt profiles and a Shirley background, where necessary. The width of the Lorentzian component in the Voigt function was fixed to the S $1s^{-1}$ core-hole lifetime broadening of 0.59 eV [33]. At photon energies close to $E_\gamma^{\rm ref}$, the Auger electron spectra were fitted with asymmetric PCI profiles based on Ref. [19].

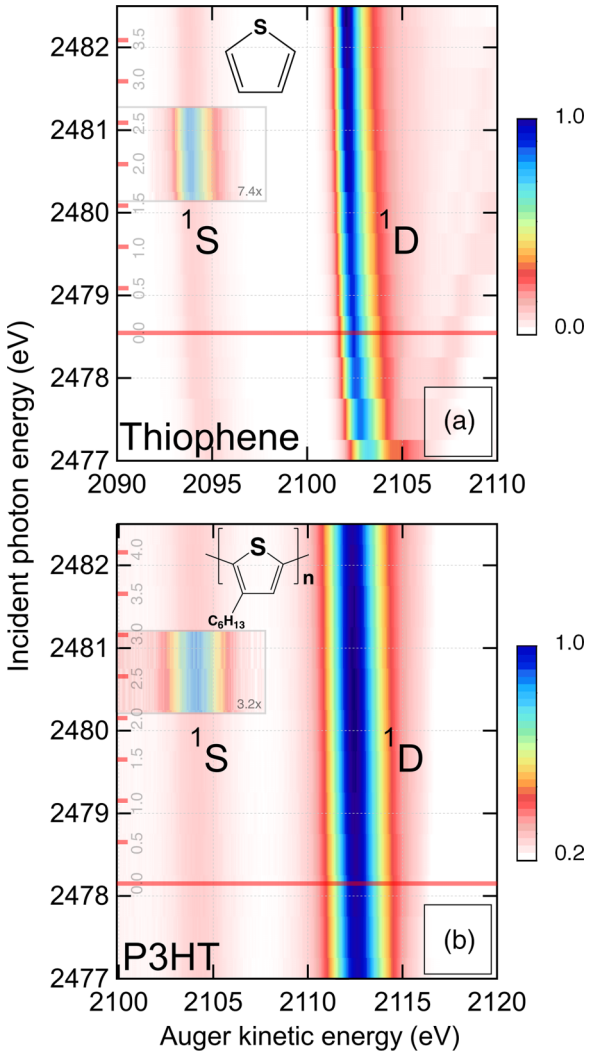

FIG. 1. 2D maps of S $KL_{2,3}L_{2,3}$ Auger spectra recorded in (a) : thiophene, (b) : P3HT. Red horizontal lines show the reference photon energy $E_\gamma^{\rm ref}$, where the excess energy $E_0 = 0$ eV. Multiplet lines corresponding to the ^1S and ^1D terms of the $2p^{-2}$ final-state configuration are labeled in the 2D maps. Red ticks and adjacent labels correspond to the E_0 scale. Insets show the ^1S term with intensity scaled by a factor of 7.4 and 3.2 for thiophene and P3HT, respectively.

IV. RESULTS AND DISCUSSION

The S $KL_{2,3}L_{2,3}$ Auger spectra for thiophene and P3HT are presented in Fig. 1 as 2D maps showing Auger electron kinetic energies as a function of the incident photon energy. The intensity is represented by a color scale. The maps are normalized to the integrated intensity. In PTC, the measurements were limited to selected photon energies, which explains the

TABLE I. Position of the S $KL_{2,3}L_{2,3}(^1D)$ spectral line in the Auger electron spectra in thiophene, P3HT and PTC, measured at high excess photon energy E_0 where PCI shifts are absent. Uncertainties in E_0 and E_{kinetic} estimated from photon and kinetic energy calibration procedures.

Sample	E_0 (eV)	E_{kinetic} (eV)
Thiophene	1000.0(3)	2101.60(1)
P3HT	1000.0(3)	2111.80(1)
PTC	200.0(3)	2111.90(1)

absence of a 2D map. The shown Auger spectra were recorded at photon energies varying with a step of 0.5 eV around the reference photon energy E_γ^{ref}, which is marked on the maps with a red horizontal line. The Auger spectra observed at the photon energies below E_γ^{ref} correspond to the relaxation of the intermediate states resulting from resonant excitation to the densely lying unoccupied orbitals, which in the case of polymers form a conduction band. In Fig. 1(b), the Auger electron kinetic energy is shown with respect to the FL as in the previously reported Auger S KLL spectra in P3HT [53]. The S KLL Auger spectrum consists of three multiplet lines corresponding to the ^1S, ^1D, and ^3P (not shown in the maps due to low intensity) terms of $2p^{-2}$ final-state configuration. Our analysis is focused on the strongest $2p^{-2}(^1D)$ multiplet line. We expect identical results for the less intense $2p^{-2}(^1S)$ and $2p^{-2}(^3P)$ lines.

The PCI effect can be observed in the 2D maps as a distinctive blueshift of the $2p^{-2}(^1D)$ spectral line as the photon energy decreases and approaches E_γ^{ref}. The S KLL Auger spectra zoomed in around the $2p^{-2}(^1D)$ line are shown in Fig. 2 for thiophene, P3HT and PTC for selected excess photon energies. Again, the Auger electron kinetic energy of the polymers is shown with respect to the FL. The black vertical dashed line marks the maximum of the $2p^{-2}(^1D)$ line in the Auger spectra measured at high E_0 values, where alteration induced by the PCI effect is absent (see Table I for the position of the black lines). Red vertical dashed lines show the $2p^{-2}(^1D)$ spectral line maximum in the spectra measured at the lowest E_0 value for each system, where the line distortion and magnitude of the PCI shift ΔE are the largest. In the following, the Auger electron kinetic energy values summarized in Table I will serve as a reference for calculating the PCI shift with respect to the unshifted spectral line. In thiophene [Fig. 2(a)], we observe the PCI-induced distortion of the Auger line, resulting in a strong asymmetry toward high kinetic energies as the E_0 decreases. This distortion is less pronounced in P3HT and PTC [Figs. 2(b) and 2(c)], which is probably related to the significant inhomogeneous broadening of the Auger line in the polymer samples compared to the gaseous thiophene.

The PCI shift ΔE observed at the lowest E_0 value with respect to the position of the unshifted Auger line (marked by the black dashed line), has approximately the same magnitude in thiophene ($\Delta E = 0.7$ eV) and in both polymers ($\Delta E =$ 0.8 eV and 0.7 eV for P3HT and PTC, respectively). However, the evolution of the PCI shift with the excess photon energy E_0 is different. In thiophene, at $E_0 = 120$ eV and above, the

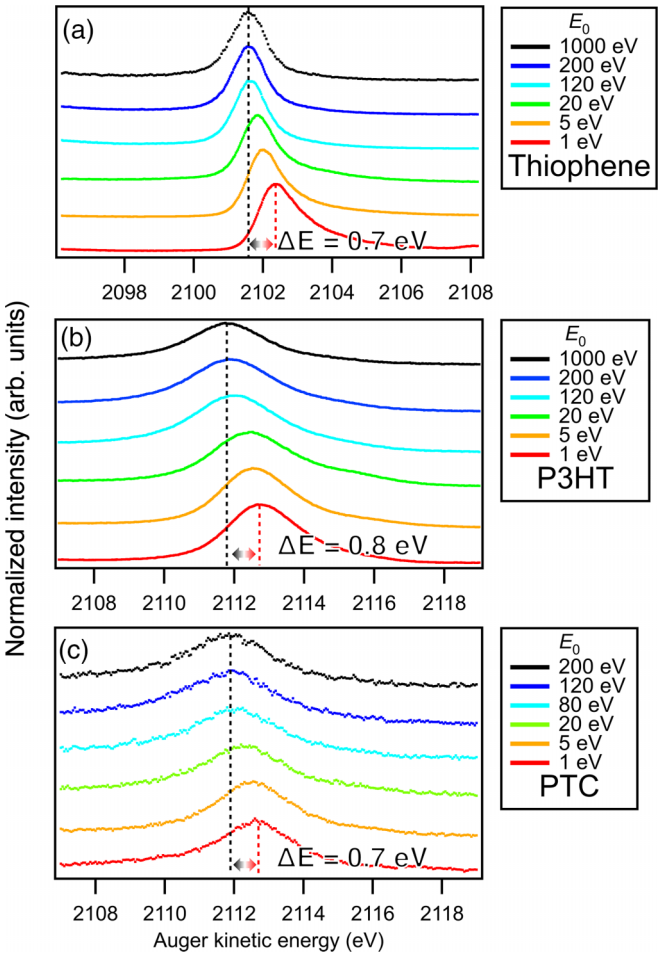

FIG. 2. Experimental S $KL_{2,3}L_{2,3}(^1D)$ Auger line profiles for selected excess photon energies E_0 for thiophene (a), P3HT (b), and PTC (c). Vertical dashed lines show the position of the spectral line at the highest (black) and at the lowest (red) values of E_0. The magnitude of the PCI shift measured at the lowest E_0 value is shown for each system.

asymmetry is imperceptible, and the line shift is close to zero. In contrast, in P3HT and PTC, the PCI shift is still appreciable at $E_0 = 120$ eV.

The experimentally measured PCI shift of the S $KL_{2,3}L_{2,3}(^1D)$ Auger line ΔE as a function of excess photon energy in thiophene, P3HT, and PTC is shown in Fig. 3 together with the theoretical results obtained within the eikonal approximation outlined above. Error bars correspond to the statistical error with a confidence interval of 95%. The inset shows the $E_0 = 0$ –25 eV range in greater detail. Remarkably, apart from the threshold energy region, both P3HT and PTC polymers clearly show a stronger PCI line shift compared to the gas-phase thiophene molecule up to $E_0 = 150$ eV. At higher excess photon energies, ΔE gradually converges to zero for all systems. A close proximity of the results for the two polymer samples can be attributed to their similar density and dielectric permittivity. Different morphology of the samples in the form of powder (PTC) and a film (P3HT) has no apparent effect on the PCI shift.

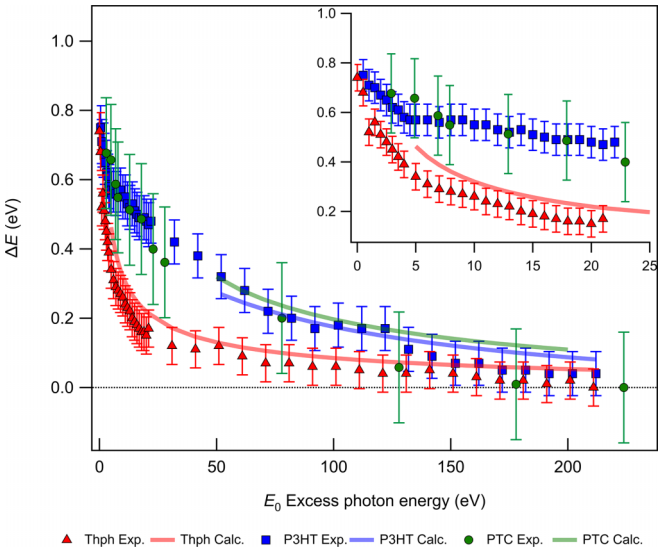

FIG. 3. Measured (thiophene: red filled triangles, P3HT: blue filled squares, PTC: green filled circles) and calculated (red continuous lines for thiophene, blue for P3HT, green for PTC) PCI shift of the S $KL_{2,3}L_{2,3}(^1D)$ Auger line ΔE as a function of excess photon energy above the S 1s ionization threshold. Horizontal dotted line corresponds to $\Delta E = 0$. The inset shows the 0–25 eV range in detail. Error bars on measured data correspond to statistical error with a confidence interval of 95%.

Theoretical results obtained using Eq. (2) for thiophene (continuous red line) and Eq. (5) for P3HT (continuous blue line) and PTC (continuous green line) are shown in Fig. 3. A very good overall agreement between the experimental data and the theoretical results is observed.

For gas-phase thiophene, the divergence from the experiment visible at $E_0 < 10$ eV (see inset), is related to the limitation of the eikonal approximation close to the ionization threshold (see Ref. [1] and discussion in Sec. II), and therefore we do not show calculations below $E_0 = 5$ eV. Nevertheless, a reasonable agreement at higher E_0, demonstrates the validity of our model using the eikonal approximation for the PCI effect in relatively large organic molecules.

Regarding the polymers, the calculations are limited to the $E_0 > 50$ eV range due to a limitation imposed by the NIST Electron Effective-Attenuation-Length Database tools [43,44]. Nonetheless, excellent agreement obtained at the accessible range of excess photon energies corroborates our model proposed to describe the PCI effect in a solid medium [see Eq. (5)].

Propagation of a slow photoelectron in the polymers is strongly influenced by elastic scattering affecting the electron trajectory and thus reducing the distance that it can travel before the Auger decay occurs. Furthermore, inelastic scattering may lead to electron energy loss. Both types of scattering result in the enhancement of the PCI effect. On the other hand, the dielectric medium efficiently screens the electron charges and thus affects the Coulomb interaction between the photoelectron and the Auger electron, leading to a reduction of the PCI effect. Therefore, the resulting PCI shift depends on the interplay of the two competing effects of the solid environment on the interacting electrons.

The PCI shift observed in the $10 \lesssim E_0 \lesssim 120$ eV region is on average approximately two times larger in the polymers than in thiophene molecule. According to Eqs. (2) and (5), amplification is given by the ratio $(\Gamma_a + \Gamma_d)/\Gamma_a\varepsilon$. On the one hand, the damping width Γ_d is in the order of ∼7–8 eV over the considered E_0 region, whereas Γ_a=0.59 eV, leading to PCI shift amplification by about a factor of 13 due to electron scattering. On the other hand, dielectric screening reduces the shift by a factor of 6.5. A combination of both effects ultimately doubles the PCI shift in polymers.

At $E_0 < 10$ eV, the difference between the PCI energy shifts in polymers and the molecule decreases and eventually disappears at the photoionization threshold. Despite the lack of calculations for EAL and the corresponding values of Γ_d for $E_0 < 50$ eV, the observed trend implies a reduction of the electron damping width Γ_d in this energy region.

A strong reduction of the PCI effect previously observed in XPS spectra of rare-gas clusters, compared to the isolated atoms, was interpreted by dielectric screening of the electron charge propagating in the cluster bulk [10]. However, a possible effect of electron scattering on the PCI effect had not been considered. One can assume that in a relatively small-size medium such as clusters with mean size $\langle N \rangle \approx 1600$ as considered in Ref. [10], photoelectron scattering does not play an essential role for the PCI shift, whereas polarization screening has a dominant effect on PCI. In contrast, in extended solid media, such as the polymers considered in our paper, both elastic and inelastic electron scattering play a preponderant role in the PCI effect and overtake the diminishing effect that polarization screening may have.

V. CONCLUSION

In this paper, we present an investigation coupling experimental and theoretical results of the PCI effect in thiophene and thiophene-based polymers. We have studied the S $KL_{2,3}L_{2,3}$ Auger decay spectra in gaseous thiophene and in solid-state organic polymers polythiophene and poly(3-hexylthiophene-2,5-diyl).

The PCI between Auger electron, photoelectron, and residual doubly charged ions has been observed in all samples. The interaction manifested itself as a significant distortion and a blueshift of the Auger spectral lines close to the ionization threshold. The PCI shift, reaching a value close to ∼1 eV just above the ionization threshold, is gradually reduced with increasing photon energy. However, it remains visible up to ∼150 eV above the ionization threshold.

Furthermore, we have shown that in solid-state samples, the PCI effect is significantly larger between $10 \lesssim E_0 \lesssim 120$ eV compared to the gas-phase molecule. We propose a model for the PCI in condensed matter, based on the eikonal approximation, which takes into account the effect of the polarization screening of the electron charges in the dielectric medium and the effect of photoelectron scattering. While the dielectric permittivity of the medium screens the electron charges and reduces the PCI effect, electron scattering counterbalances this reduction, decreasing the travel distance of a slow photoelectron in the medium, thus enhancing the PCI effect.

Apart from these findings, very good agreement between experimental and theoretical results in thiophene demonstrates the validity of the eikonal approximation for the PCI description in relatively large organic molecules.

Our paper paves the way toward future investigations of the interplay between charge screening and electron scattering for PCI in various media. The general nature of the PCI effect, showcased in our paper in an isolated organic molecule and in solid organic polymers, calls for further studies of PCI in cluster, liquid, and solid media.

ACKNOWLEDGMENTS

Experiments were performed on the GALAXIES beamline at SOLEIL Synchrotron, France (Proposals No. 99200174, No. 99210051, and No. 20201715). We are grateful to the SOLEIL staff for their smooth operation of the facility. R.P. gratefully acknowledges fruitful discussions with Dr. C. Gahl. N.V. and T.M. acknowledge funding from the European Research Council Horizon 2020 research and innovation program under Marie Skłodowska-Curie Grant Agreement No. No [860553]. J.B.M. and T.M. acknowledge financial support from the French Agence Nationale de la Recherche (ANR) through the ATTOMEMUCHO project (No. ANR-16-CE30-0001). D.K. wishes to acknowledge financial support from LabEx MiChem, France.

APPENDIX: ELECTRON EFFECTIVE ATTENUATION LENGTH

To calculate the electron EAL [L in Eq. (3)] [55], we used the NIST Standard Reference Database tools 71 and 82 [43,44].

To describe photoelectron scattering within the polymer media, the EAL calculations account for both inelastic and elastic scattering contributions. Inelastic scattering enters the EAL in the form of the inelastic mean free path (IMFP), the average distance between successive inelastic collisions of an electron moving in a medium with a given energy [56]. Elastic scattering enters the EAL as the transport mean free path (TMFP), the average distance that the electron must travel before its momentum in the initial direction of the motion is reduced, by elastic scattering alone, to $1/e$ of its initial value [57]. As an example, in Table II we show IMFP and TMFP values for both P3HT and PTC calculated at a photoelectron kinetic energy of 50 eV.

TABLE II. IMFP and TMFP values for P3HT and PTC calculated at a photoelectron kinetic energy of 50 eV.

Sample	IMFP (Å)	TMFP (Å)
P3HT	4.2	6.6
PTC	3.9	6.9

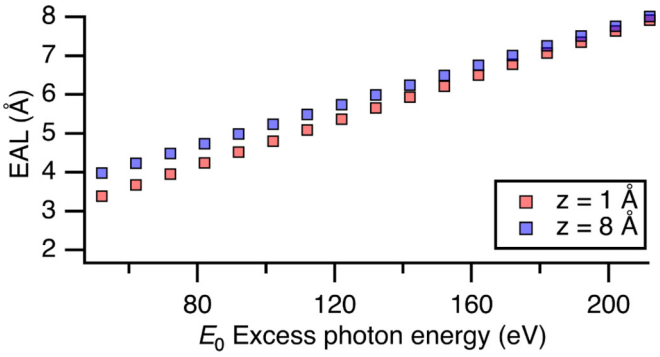

FIG. 4. EAL as a function of photoelectron kinetic energy calculated for P3HT at $z = 1$ Å (orange squares) and $z = 8$ Å (purple squares).

The EAL depends on the depth from the surface into the material z, electron emission angle with respect to the surface normal α, IMFP, and TMFP.

Figure 4 shows a dependence of the EAL on the photoelectron kinetic energy calculated for P3HT at $z = 1$Å, and $z = 8$Å. The former depth value was also used in the calculations shown in Fig. 3. The NIST tools set a limitation of 50 eV as a bottom threshold for the electron kinetic energy. This is because the relativistic TPP-2M (Tanuma, Powell and Penn) equation used to simulate the IMFP is not reliable in the optical range below 50 eV [58]. EAL values were calculated within the ∼50–200 eV photoelectron kinetic energy range, corresponding to the excess photon energy E_0. Sampling was done every ∼10 eV. The input parameters include the atom fraction of polymer component, the number of valence electrons, band gap, and density. The atom fractions used are H = 0.56, C = 0.4, and S = 0.04, and a density = 1.1 g/cm^3 [59]. The number of valence electrons was set to 2 and the band gap was set to 2 eV [60].

To demonstrate how each parameter affects the PCI shift, Fig. 5 shows ΔE and its dependence on z and ε for P3HT.

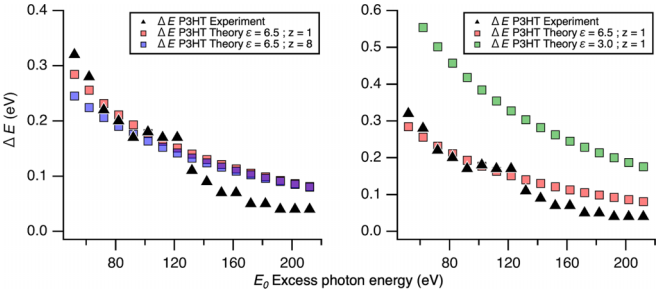

FIG. 5. Left: Calculated PCI shift for P3HT at $z = 1$ Å(orange squares), $z = 8$ Å (purple squares). Right: Calculated PCI shift for P3HT at $\varepsilon = 3$ (green squares), $\varepsilon = 6.5$ (orange squares). Experimental data in black triangles.

[1] M. Kuchiev and S. Sheinerman, Post-collision interaction in atomic processes, Sov. Phys. Usp. **32**, 569 (1989).

[2] V. Schmidt, Photoionization of atoms using synchrotron radiation, Rep. Prog. Phys. **55**, 1483 (1992).

[3] D. L. Hansen, G. B. Armen, M. E. Arrasate, J. Cotter, G. R. Fisher, K. T. Leung, J. C. Levin, R. Martin, P. Neill, R. C. C. Perera, I. A. Sellin, M. Simon, Y. Uehara, B. Vanderford, S. B. Whitfield, and D. W. Lindle, Postcollision-interaction effects in HCl following photofragmentation near the chlorine K edge, Phys. Rev. A **57**, R4090(R) (1998).

[4] D. L. Hansen, W. C. Stolte, O. Hemmers, R. Guillemin, and D. W. Lindle, Anion formation moderated by post-collision interaction following core-level photoexcitation of CO, J. Phys. B: At., Mol. Opt. Phys. **35**, L381 (2002).

[5] M. K. Odling-Smee, E. Sokell, A. A. Wills, and P. Hammond, Observation of post-collision interaction (PCI) in HBr using two-dimensional photoelectron spectroscopy, J. Phys. B: At., Mol. Opt. Phys. **32**, 2529 (1999).

[6] C. Bomme, R. Guillemin, S. Sheinerman, T. Marin, L. Journel, T. Marchenko, R. K. Kushawaha, N. Trcera, M. N. Piancastelli, and M. Simon, Post-collision interaction manifestation in molecular systems probed by photoelectron-molecular ion coincidences, J. Phys. B: At. Mol. Opt. Phys. **46**, 215101 (2013).

[7] T. Miller and T.-C. Chiang, Solid-state screening effect on the post-collision interaction, Phys. Rev. B **29**, 1121 (1984).

[8] V. M. Mikushkin, A. V. Zakharevich, I. I. Pavletsov, S. E. Sysoev, V. V. Shnitov, M. Y. Kuchiev, and S. A. Sheinerman, Postcollision interaction in the excitation of a gold 4d vacancy by fast electrons, JETP Lett. **58**, 891 (1993).

[9] B. Kassühlke, R. Romberg, P. Averkamp, and P. Feulner, Substrate Mediated Suppression of Postcollision Interaction Effects, Phys. Rev. Lett. **81**, 2771 (1998).

[10] A. Lindblad, R. F. Fink, H. Bergersen, M. Lundwall, T. Rander, R. Feifel, G. Öhrwall, M. Tchaplyguine, U. Hergenhahn, S. Svensson, and O. Björneholm, Postcollision interaction in noble gas clusters: Observation of differences in surface and bulk line shapes, J. Chem. Phys. **123**, 211101 (2005).

[11] D. Coward and S. Thurgate, Post collision interaction in the L_3M_4, $_5M_4$, $_5$ Auger spectra in solid state copper, J. Electron Spectrosc. Relat. Phenom. **107**, 193 (2000).

[12] T. Miteva, N. V. Kryzhevoi, N. Sisourat, C. Nicolas, W. Pokapanich, T. Saisopa, P. Songsiriritthigul, Y. Rattanachai, A. Dreuw, J. Wenzel, J. Palaudoux, G. Öhrwall, R. Puttner, L. S. Cederbaum, J.-P. Rueff, and D. Céolin, The all-seeing eye of resonant auger electron spectroscopy: A study on aqueous solution using tender x-rays, J. Phys. Chem. Lett. **9**, 4457 (2018).

[13] H. W. Berry, Energy distribution of electrons from ionizing collisions of heavy particles, Phys. Rev. **121**, 1714 (1961).

[14] R. B. Barker and H. W. Berry, Electron energy distributions from ionizing collisions of helium and neon ions with helium, Phys. Rev. **151**, 14 (1966).

[15] G. N. Ogurtsov, Auger line shift due to the post-collision interaction at large excess energies, J. Phys. B **16**, L745 (1983).

[16] A. Niehaus, Analysis of post-collision interactions in Auger processes following near-threshold inner-shell photoionization, J. Phys. B: At. Mol. Phys. **10**, 1845 (1977).

[17] K. Helenelund, S. Hedman, L. Asplund, U. Gelius, and K. Siegbahn, An improved model for post-collision interaction (PCI) and high resolution ar LMM auger spectra revealing new PCI effects, Phys. Scr. **27**, 245 (1983).

[18] A. Russek and W. Mehlhorn, Post-collision interaction and the auger lineshape, J. Phys. B **19**, 911 (1986).

[19] P. Straten, R. Morgenstern, and A. Niehaus, Angular dependent post-collision interaction in auger processes, Z. Phys. D: At., Mol. Clusters **8**, 35 (1988).

[20] M. Y. Kuchiev and S. A. Sheinerman, Resonant processes involving the production of three charged particles, Sov. Phys. JETP **63**, 986 (1986).

[21] G. B. Armen, J. Tulkki, T. Aberg, and B. Crasemann, Quantum theory of post-collision interaction in inner-shell photoionization: Final-state interaction between two continuum electrons, Phys. Rev. A **36**, 5606 (1987).

[22] A. K. Kazansky and N. M. Kabachnik, Nonstationary theory for short-pulse near-threshold photoionization of inner atomic shells, Phys. Rev. A **72**, 052714 (2005).

[23] R. Guillemin, S. Sheinerman, C. Bomme, L. Journel, T. Marin, T. Marchenko, R. K. Kushawaha, N. Trcera, M. N. Piancastelli, and M. Simon, Ultrafast Dynamics in Postcollision Interaction After Multiple Auger Decays in Argon 1 s Photoionization, Phys. Rev. Lett. **109**, 013001 (2012).

[24] R. Guillemin, S. Sheinerman, R. Puttner, T. Marchenko, G. Goldsztejn, L. Journel, R. K. Kushawaha, D. Céolin, M. N. Piancastelli, and M. Simon, Postcollision interaction effects in K L L Auger spectra following argon 1 s photoionization, Phys. Rev. A **92**, 012503 (2015).

[25] H. Kjeldsen, T. D. Thomas, P. Lablanquie, M. Lavollée, F. Penent, M. Hochlaf, and R. I. Hall, Post-collision interaction effects in near-threshold Ar -shell photoionization, J. Phys. B: At. Mol. Opt. Phys. **29**, 1689 (1996).

[26] F. Penent, J. Palaudoux, P. Lablanquie, L. Andric, R. Feifel, and J. H. D. Eland, Multielectron Spectroscopy: The Xenon 4*d* Hole Double Auger Decay, Phys. Rev. Lett. **95**, 083002 (2005).

[27] R. Guillemin, L. Gerchikov, S. Sheinerman, M. Zmerli, T. Marin, L. Journel, O. Travnikova, T. Marchenko, B. Lassalle-Kaiser, M. N. Piancastelli, and M. Simon, Photoelectron-Auger-electron angular-momentum transfer in core-ionized Ar: Beyond the standard post-collision-interaction model, Phys. Rev. A **99**, 063409 (2019).

[28] P. Lablanquie, S. Sheinerman, F. Penent, T. Aoto, Y. Hikosaka, and K. Ito, Dynamics of double photoionization near the Ar 2p threshold investigated by threshold electron–auger electron coincidence spectroscopy, J. Phys. B: At., Mol. Opt. Phys. **38**, L9 (2005).

[29] A. J. Heeger, Nobel Lecture: Semiconducting and metallic polymers: The fourth generation of polymeric materials, Rev. Mod. Phys. **73**, 681 (2001).

[30] R. Valaski, C. Canestraro, L. Micaroni, R. Mello, and L. Roman, Organic photovoltaic devices based on polythiophene films electrodeposited on FTO substrates, Sol. Energy Mater. Sol. Cells **91**, 684 (2007).

[31] E. Nasybulin, J. Feinstein, M. Cox, I. Kymissis, and K. Levon, Electrochemically prepared polymer solar cell by three-layer deposition of poly(3,4-ethylenedioxythiophene)/poly(2,2-bithiophene)/fullerene (PEDOT/PBT/C60), Polymer **52**, 3627 (2011).

[32] K.-J. Baeg, D. Khim, D.-Y. Kim, J. B. Koo, I.-K. You, W. S. Choi, and Y.-Y. Noh, High mobility top-gated poly(3-hexylthiophene) field-effect transistors with high work-function Pt electrodes, Thin Solid Films **518**, 4024 (2010).

[33] M. O. Krause and J. H. Oliver, Natural widths of atomic *K* and *L* levels, *Kα* X-ray lines and several *KLL* Auger lines, J. Phys. Chem. Ref. Data **8**, 329 (1979).

[34] S. Sheinerman, P. Lablanquie, F. Penent, J. Palaudoux, J. H. D. Eland, T. Aoto, Y. Hikosaka, and K. Ito, Electron correlation in Xe 4d auger decay studied by slow photoelectron–auger electron coincidence spectroscopy, J. Phys. B: At., Mol. Opt. Phys. **39**, 1017 (2006).

[35] M. P. Hughes, K. D. Rosenthal, N. A. Ran, M. Seifrid, G. C. Bazan, and T. Nguyen, Determining the dielectric constants of organic photovoltaic materials using impedance spectroscopy, Adv. Funct. Mater. **28**, 1801542 (2018).

[36] M. Böckmann, T. Schemme, D. H. de Jong, C. Denz, A. Heuer, and N. L. Doltsinis, Structure of P3HT crystals, thin films, and solutions by UV/Vis spectral analysis, Phys. Chem. Chem. Phys. **17**, 28616 (2015).

[37] R. Singh, J. Kumar, R. K. Singh, R. C. Rastogi, and V. Kumar, Low frequency ac conduction and dielectric relaxation in pristine poly(3-octylthiophene) films, New J. Phys. **9**, 40 (2007).

[38] M. Estrada, I. Mejia, A. Cerdeira, and B. Iñiguez, MIS polymeric structures and OTFTs using PMMA on P3HT layers, Solid-State Electron. **52**, 53 (2008).

[39] M. Okutan, Y. Yerli, S. E. San, F. Yilmaz, O. Günaydin, and M. Durak, Dielectric properties of thiophene based conducting polymers, Synth. Met. **157**, 368 (2007).

[40] O. Travnikova, M. Patanen, J. Söderström, A. Lindblad, J. J. Kas, F. D. Vila, D. Céolin, T. Marchenko, G. Goldsztejn, R. Guillemin, L. Journel, T. X. Carroll, K. J. Børve, P. Decleva, J. J. Rehr, N. Mårtensson, M. Simon, S. Svensson, and L. J. Sæthre, Energy-dependent relative cross sections in carbon 1s photoionization: Separation of direct shake and inelastic scattering effects in single molecules, J. Phys. Chem. A **123**, 7619 (2019), pMID: 31386367.

[41] C. Menendez and F. Guinea, Electron-phonon scattering in polyparaphenylene, Phys. Rev. B **28**, 2183 (1983).

[42] R. Mansfield, Impurity Scattering in Semiconductors, Proc. Phys. Soc. London, Sect. B **69**, 76 (1956).

[43] A. Jablonski, NIST Electron Inelastic-Mean-Free-Path Database—Version 1.2 (2010)

[44] A. Jablonski, NIST Electron Effective-Attenuation-Length Database—Version 1.3 (2011)

[45] J.-P. Rueff, J. M. Ablett, D. Céolin, D. Prieur, T. Moreno, V. Balédent, B. Lassalle-Kaiser, J. E. Rault, M. Simon, and A. Shukla, The GALAXIES beamline at the SOLEIL synchrotron: Inelastic X-ray scattering and photoelectron spectroscopy in the hard X-ray range, J. Synchrotron Radiat. **22**, 175 (2015).

[46] D. Céolin, J. Ablett, D. Prieur, T. Moreno, J.-P. Rueff, T. Marchenko, L. Journel, R. Guillemin, B. Pilette, T. Marin, and M. Simon, Hard X-ray photoelectron spectroscopy on the GALAXIES beamline at the SOLEIL synchrotron, J. Electron Spectrosc. Relat. Phenom. **190**, 188 (2013).

[47] G. Vereecke and P. G. Rouxhet, Surface charging of insulating samples in x-ray photoelectron spectroscopy, Surf. Interface Anal. **26**, 490 (1998).

[48] L. Avaldi, G. Dawber, R. Camilloni, G. C. King, M. Roper, M. R. F. Siggel, G. Stefani, and M. Zitnik, Near-threshold photoionization of the Ar 2p subshell, J. Phys. B: At. Mol. Opt. Phys. **27**, 3953 (1994).

[49] M. Breinig, M. H. Chen, G. E. Ice, F. Parente, B. Crasemann, and G. S. Brown, Atomic inner-shell level energies determined by absorption spectrometry with synchrotron radiation, Phys. Rev. A **22**, 520 (1980).

[50] G. Greczynski and L. Hultman, X-ray photoelectron spectroscopy: Towards reliable binding energy referencing, Prog. Mater. Sci. **107**, 100591 (2020).

[51] A. P. Hitchcock, J. A. Horsley, and J. Stöhr, Inner shell excitation of thiophene and thiolane: Gas, solid, and monolayer states, J. Chem. Phys. **85**, 4835 (1986).

[52] C. Arantes, B. G. A. L. Borges, B. Beck, G. Araújo, L. S. Roman, and M. L. M. Rocco, Femtosecond electron delocalization in poly(thiophene) probed by resonant Auger spectroscopy, J. Phys. Chem. C **117**, 8208 (2013).

[53] Y. Garcia-Basabe, D. Ceolin, A. J. G. Zarbin, L. S. Roman, and M. L. M. Rocco, Ultrafast interface charge transfer dynamics on P3HT/MWCNT nanocomposites probed by resonant Auger spectroscopy, RSC Adv. **8**, 26416 (2018).

[54] E. Kukk, Spectrum Analysis by Curve Fitting (SPANCF) Macro Package for Igor Pro (2009).

[55] A. Jablonski, The electron attenuation length revisited, Surf. Sci. Rep. **47**, 33 (2002).

[56] D.-N. Le and H. T. Nguyen-Truong, Analytical Formula for the Electron Inelastic Mean Free Path, J. Phys. Chem. C **125**, 18946 (2021).

[57] A. Jablonski, Transport cross section for electrons at energies of surface-sensitive spectroscopies, Phys. Rev. B **58**, 16470 (1998).

[58] S. Tanuma, C. J. Powell, and D. R. Penn, Calculations of electron inelastic mean free paths. V. Data for 14 organic compounds over the 50-2000 eV range, Surf. Interface Anal. **21**, 165 (1994).

[59] N. Vukmirović and L.-W. Wang, Electronic structure of disordered conjugated polymers: Polythiophenes, J. Phys. Chem. B **113**, 409 (2009).

[60] M. A. Ansari, S. Mohiuddin, F. Kandemirli, and M. I. Malik, Synthesis and characterization of poly(3-hexylthiophene): improvement of regioregularity and energy band gap, RSC Adv. **8**, 8319 (2018).